Observation of high-temperature magnetic transition and existence of ferromagnetic short-range correlations above transition in La_2FeMnO_6

Jasnamol P P[1, 2], P Neenu Lekshmi[2], Senoy Thomas[2], K G Suresh[3] and Manoj Raama Varma[1, 2]
[1]Academy of Scientific and Innovative Research (AcSIR), CSIR- National Institute for Interdisciplinary Science and Technology (CSIR-NIIST) Campus, Thiruvananthapuram-695 019, India.
[2]Materials Science and Technology Division, CSIR- National Institute for Interdisciplinary Science and Technology (CSIR-NIIST), Thiruvananthapuram-695 019, India.
[3]Department of Physics, Indian Institute of Technology Bombay, Mumbai 400 076, India.
E-mail: manoj@niist.res.in

We present the observation of a high-temperature magnetic transition along with ferromagnetic short-range correlations (FSCs) in La_2FeMnO_6 perovskite system. XPS analysis confirmed the presence of Fe^{+3} and Mn^{+3} cations. The M-T curves show two distinct transitions at T_{C1}~60 K and T_C~425 K. Coercivity values of ~1140 Oe, and ~35 Oe are observed at 2 K and 300 K respectively. The thermomagnetic analysis reveals the presence of FSCs in La_2FeMnO_6 up to T^*= 570 K, well above the transition point, similar to Griffiths-like phase (GP). The presence of ferromagnetic clusters in the paramagnetic region might be due to the intrinsic inhomogeneities associated with the structure, quenched disorder related to the B-site cations and the antisite boundaries. The coefficient of lower temperature electronic specific heat is as high as 59.5 $mJmol^{-1}K^{-2}$. The electron spin resonance spectra show ferromagnetic resonance signals that are pointing to the possibility of the presence of FSCs at room temperature. The material seems to be a quite promising candidate for some room temperature applications due to the possibility of coexistence of functionalities like ferromagnetism, ferrimagnetism, GP, magnetotransport coupling, etc. in a single material.

Double perovskite, High temperature transition, Ferromagnetic short-range correlations, Specific heat, Electron spin resonance, Ferromagnetic resonance signals.

Introduction

The perovskite oxides ABO_3 (A = alkaline or rare earth elements (R), B =transition elements) possess a vast variety of physical properties like ferromagnetism (FM), ferrimagnetism (FiM), half metallicity, magnetoresistance, magnetodielectric (MD) coupling, etc. [1-10] The manganite perovskites ($AMnO_3$) have received considerable attention due to their magnetic, transport and magnetotransport properties linked with the change in the spin state.[11-12] Introducing a second element to the B-site will provide further characteristics to the system [Double Perovskite (DP)] in accordance with the difference in cationic ordering, oxidation states, antiphase boundaries, multiple exchange interactions, lattice distortion, etc.[1-4] Enormous studies are being carried out in nowadays on rare earth (RE) manganites with DP structure that exhibit multifunctional properties by virtue of their wide B/Mn cationic range.[7-10] Among these compounds, La_2NiMnO_6 is quite attractive because it is a FM semiconductor with good magnetodielectricity and magnetoresistance at temperatures cose to room temperature due to its frustrated spin system originating from Ni and Mn cations.[13-14] Among the RE manganites, La_2FeMnO_6, the Fe counterpart of La_2NiMnO_6, remains unexplored fully, to a large extent.

The perovskites $LaFeO_3$ and $LaMnO_3$ are antiferromagnetic (AFM) insulators in bulk form with Néel temperature (T_N) 740 K and 140 K respectively, in which the superexchange interactions Fe^{3+}-O-Fe^{3+} and Mn^{3+}-O-Mn^{3+} lead to AFM coupling.[15-17] There are reports pertaining to the preparation of La_2FeMnO_6 having perovskite structure.[18-19] Many researchers continued the work on La_2FeMnO_6 both experimentally and theoretically, but a clear magnetic transition was not identified experimentally on bulk La_2FeMnO_6. The present work presents the observation of a high-temperature magnetic transition and the evidence for the existence of ferromagnetic short-range correlations (FSCs) far above room temperature in La_2FeMnO_6.

Experimental

Polycrystalline La_2FeMnO_6 is synthesized by employing Pechini method.[19] High purity chemicals $La(NO_3)_3.6H_2O$, $Fe(NO_3)_3.9H_2O$ and $Mn(NO_3)_2$ (Sigma-Aldrich, purity ~99.99%) were weighed according to stoichiometry. Citric acid was added to this mixture such that the citric acid and cation ratio is 1:3. The nitrates and citric acid were mixed in 1 L beaker in de-ionized water medium at 70ºC with continuous stirring. The temperature were slowly raised and finally the combustion happened at 200ºC. The powder was kept at same condition for one day. The precursor powder was ground well and loaded into a muffle furnace at 600ºC for 2 hours and 900ºC for two hours. The powders were ground well and pelletized using a hydraulic press. For pelletization, polyvinyl alcohol was used as a binder. The pellets were finally sintered at 900ºC for 6 hours. The sintered pellets were ground well, and the final material was confirmed as phase pure La_2FeMnO_6 by using the X-ray diffraction (XRD) data obtained by Philips PANalytical X'Pert Pro Powder X-Ray Diffractometer with a Ni filtered Cu Kα radiation (λ=1.5406 Å). The Rietveld refinement of the XRD pattern was done using the software GSAS – EXPGUI.[20] The crystallographic structure is framed using CrystalMaker®.[21] X-ray photoelectron spectroscopy (XPS) measurements were carried out using an Omicron Nanotechnology Multiprobe Instrument. The XPS spectra corresponding to Fe 2p and Mn 2p of La_2FeMnO_6 are recorded by using a high resolution hemisphere analyzer EA 125 HR equipped with a detection system consisting of seven channeltrons. A monochromatic Al Kα source of energy, hν =1486.6 eV was used to probe the La_2FeMnO_6 pellets, attached by a double-sided tape to the molybdenum sample holder. The pressure in the XPS chamber during the measurements was 5x 10^{-10} mbar. A wide scan was collected to ensure that no foreign materials were present on the sample surface. Narrow scans of Fe 2p and Mn 2p regions were collected at analyzer pass energy of 20 eV. The peaks are fitted using the XPS Peak Fit software. The magnetization measurements were carried out on La_2FeMnO_6 powders by using a Vibrating Sample Magnetometer (VSM) attached to a Physical Property Measurement System (Dynacool, Quantum Design). The specific heat (C) is measured for the temperature range of 10-150 K by using the heat capacity option attached to the PPMS (Dynacool, Quantum Design). The electron spin resonance (ESR) spectra obtained using JES - FA200 ESR Spectrometer (ESR-JEOL, Japan) at temperatures 100 K, 170 K, and 300 K.

Results and discussion

The orthorhombic, Pbnm crystal structure is confirmed for La_2feMnO_6 by the Rietveld refinement using GSAS – EXPGUI[20] ($_{W}R_{P}$ = 4.64%). The observed, calculated and difference data are shown in Fig.1(i) and the obtained lattice parameters are, a= 5.54 Å, b=5.51 Å, c= 7.81 Å, and α, β, γ = 90° with <Fe-O-Mn> bond angle of 161.75°. The crystallographic structure framed using CrystalMaker® is shown in Fig.1(ii).

The XPS spectra corresponding to Fe 2p and Mn 2p of La_2FeMnO_6 are analyzed. The binding energies were corrected by C 1s as reference energy (C 1s = 284.8 eV). The peaks are fitted using the XPS Peak Fit software and the fitted curves are shown in Fig.1(iii) and Fig.1(iv). The fitted curves give single peak for Fe $2p_{3/2}$ and Mn $2p_{3/2}$ with peak positions at 710.14 eV and 641.36 eV respectively which confirms the oxidation states of cations as Fe^{3+} and Mn^{3+}.[22,23]

Based on the reported density-functional calculations, La_2FeMnO_6 could be either a FM semiconductor or a FM half-metal or a FM metal or a FiM semiconductor under different biaxial strain conditions.[24] Also, de Lima *et al.* reported the magnetic properties of La_2FeMnO_6 bulk with T_C=65 K and coercivity (H_C) of 1160 Oe at 2 K and 170 Oe at 300 K.[25] Further, a hysteresis loop with small H_C and remanence (M_r) at 300 K was also reported for La_2FeMnO_6.[26] In the present study, zero field cooled (ZFC) and field cooled (FC) magnetizations were measured in the temperature range 5-385 K using the cryostat (Inset of fig.2) and I the range 300-950 K using the oven (Fig.2) in applied fields of 50, 200 and 1000 Oe. The temperature dependent magnetization (M-T) show irreversibility in magnetization as can be evidenced in the ZFC and FC bifurcation at lower temperatures and lower applied fields, which points towards the presence of spin frustration/ spin glass state at lower temperatures in accordance with the previous reports on La_2FeMnO_6.[27-29] The derivative dM/dT vs. T plot (Fig.3(i))indicates a broad transition at T_{C1}=60 K, which corroborates the spin glass-like transition reported earlier.[25,27-29]

Bhame *et al.* observed a positive values of Curie-Weiss constant (Θ) as an indication of the presence of ferromagnetic exchange interactions and a H_C of 1170 Oe at 12 K for La_2FeMnO_6.[30] The M-T in the range 5-300 K is similar to that observed in previous cases, and a closer look at the plot shows that the moment does not go to zero even at room temperature.[30,31] Further, the room temperature hysteresis loop is also reported for La_2FeMnO_6.[25, 26] Ueda *et al.* observed no transition in the M-T in the range of 50-400 K, and predicted that there might be an AFM transition above 400 K.[33] They have also fabricated thin films of La_2FeMnO_6, by artificially creating superlattices and by natural growth and showed a FM to PM transition (T_C) at ~230 K and ~380 K respectively.[32,33]

This instigated us to carry out higher temperature (300-950 K) M-T measurements (Fig.2), which showed a transition at T_C~425 K as shown in dM/dT vs. T plot (Fig.3(ii)). This evidence of the onset of a magnetic transition above room temperature is in line with the theoretical predictions and experimental observations in La_2FeMnO_6 thin films.[34-35] The disordered cation arrangements generate antisite boundaries leading to competing exchange interactions viz. Fe^{3+}-O-Mn^{3+} FiM interactions, Fe^{3+}-O-Fe^{3+}, and Mn^{3+}–O–Mn^{3+} AFM interactions and Mn^{3+}–O–Mn^{3+} dynamic FM interactions.[17, 26] Further, there is a key role played by the <B-O-B'> bond angle in determining the exchange interaction strength with the maximum in exchange interaction for 180°. The super exchange interaction is rather favored in this case since the <Fe-O-Mn> bond angle is as high as 161.75°.

Field dependent isothermal magnetization (M-H) was measured in the field range of -90 kOe to +90 kOe at different temperatures ranging from 2 to 950 K, and representative results are summarized in Fig.3(iii). The M-H is non-saturating even at the highest field due to the inhomogeneities associated with its structure. Variations of H_C and M_r with temperature are shown in Fig.3(iv). It shows a hysteresis with H_C=1140 Oe and M_r=7.8 emu/g at 2 K and H_C=35 Oe and M_r=0.2 emu/g at 300 K that are in agreement with the earlier report[25,30] and the loop disappears at higher temperatures. The room temperature loop is almost similar to that reported earlier.[25, 26] The coercivity value of 1140 Oe drops to 215 Oe as the sample is warmed to 50 K from 2 K and then a slow rate of decrease in H_C with temperature is observed, which is an indication of the decrease of the strength of FM clusters and increase of the strength of PM matrix. The straight line plot at 950 K, with no H_C, and M_r, shows the complete PM state. The M-H curves show a non-linear behavior for low fields (< 2 kOe) even above T_C, which is an indication of the presence of weak magnetization in the PM region.

The inverse susceptibility derived from FC magnetization for 20, 50, 200, 1000 Oe and 10 kOe is shown in Fig.4(i) and the fit to Curie-Weiss (CW) law $\chi = \frac{C_W}{T}$ for 20 Oe is shown in Fig.4(ii). A CW fit is obtained only above T^*=570 K and the presence of FSC is clearly evidenced bye the plot as a sharp downturn below T^*, which is gradually reduced as the field is increased. This feature is usually considered as a manifestation of typical Griffiths-like phases (GP).[36-51] GP was originally proposed as a randomly distributed Ising FM regions with nearest neighbor exchange interactions J and 0 with probabilities p and (1-p) respectively.[52] The CW fit in PM region yields an effective magnetic moment, $\mu_{eff} = 2.828\sqrt{C_w}$ (C_w is the Curie constant) as 6.5 μ_B / F.U. The XPS spectra confirmed Fe^{3+} and Mn^{3+} spin states in La_2FeMnO_6. The theoretically expected μ_{eff} for La_2FeMnO_6 with Fe^{3+} and Mn^{3+} are given in Table 1. The obtained μ_{eff} proclaims that the Fe^{3+} and Mn^{3+} are not in a low spin state (LS) simultaneously, and if spin-orbit coupling is present, Fe^{3+} should not be in LS. The FM state may arise from the high spin state (HS) Fe^{3+} (t_{2g}^3, e_g^2) and LS Mn^{3+} (t_{2g}^4, e_g^0), whereas the FiM state arises from LS Fe^{3+} (t_{2g}^5, e_g^0) and HS Mn^{3+} (t_{2g}^3, e_g^1), under certain strain conditions.[24] A recent study on La_2FeMnO_6 thin film confirmed AFM coupling of HS Fe^{3+} and HS Mn^{3+}, leading to FiM and observed an inverse relationship in between saturation magnetization and Fe/Mn-order.[34]

Table 1.

Spin-Orbit Coupling	**Mn^{3+} (HS)**	**Mn^{3+} (LS)**
Fe^{3+} (HS)	5.916	5.916
Fe^{3+} (LS)	1.732	1.732
Spin Only interaction	**Mn^{3+} (HS)**	**Mn^{3+} (LS)**
Fe^{3+} (HS)	7.681	6.16

Fe^{3+} (LS)	5.196	3.317

The disordered perovskite causes a random dilution of FM with different exchange interactions viz. superexchange and double exchange interactions as described before and causes the evolution of FSCs above T_C. The presence of inhomogeneous magnetic states, magnetic clusters and random competing exchange interactions in La_2FeMnO_6 are well reported previously.[27-30] Moreover, the quenched disorder, triggered by the random chemical replacement of ions of different sizes can also induce intrinsic inhomogeneities in manganites.[53-55] The disorder is quenched within the distorted structure of La_2FeMnO_6 due to the strong coupling of Jahn-Teller distortion of the Fe^{3+}/Mn^{3+} ions and orthorhombic crystal lattice so that the FM bonds can be assumed as fixed within the lattice that form clusters and FSCs.[54]

Usually, the susceptibility of a Griffiths-like phase in low fields follows the power law,[36-48] $\chi^{-1} \propto (T - T_C^R)^{1-\lambda}$, where λ is the magnetic susceptibility exponent ($0 \le \lambda \le 1$) and T_C^R is the random critical temperature. T_C^R is taken as the temperature for which the equation yields a λ (λ_{PM}) value close to zero above T^*. The Θ obtained from CW fit is 18 K for 20 Oe (Fig.4(ii)), and assuming T_C^R at 18 K well establishes λ_{PM}~0.02. The linear part of the plot $\ln(\chi^{-1})$ vs. $\ln(T - T_C^R)$ (Fig. 6) is fitted with the power law and estimated the susceptibility exponent λ as 0.54 at 20 Oe and 0.29 at 200 Oe. The value of λ lies in between 0 and 1 and is decreasing with increase in the field, a signature of Griffiths-like phases. [36-48] The Arrot plots (M^2 vs. H/M) at five different temperatures, below and above T_C are shown in Fig.4(iv). The linear extrapolation to the high field region of the Arrot plot gives a negative M^2 axis intercept confirming the absence of spontaneous magnetization (Fig.4(iv)) with the existence of finite-sized FM interrelated spins without any static long-range magnetization.[40-41]

The presence of inhomogeneous magnetic phases with co-existence of FM and AFM states in La_2FeMnO_6 was reported where, the FM phase originating from static Jahn–Teller distortions removed Mn^{3+}–O–Mn^{3+} dynamic interactions and the AFM phase arising from Fe^{3+}–O–Fe^{3+} interactions.[27] De *et al.* reported a glassy complex system at low temperatures with two dynamical freezing points below room temperature (at 20 K and 255 K), in La_2FeMnO_6 due to phase separation that was observed in many mixed valence manganites and also due to the existence of several competing magnetic interactions induced by antiphase boundaries[28-29] Zhou *et al.* studied $LaMn_{1-x}Fe_xO_3$ ($0<x<1.0$) system and concluded that Mn favors double exchange interaction whereas Fe favors AFM superexchange.[35] Bhame *et al.* reported the material as a spin glass, with Fe^{3+} and Mn^{3+} ions having Mn-rich and/or Fe-rich clusters of different sizes, causing predominant FM or AFM interactions respectively.[30] These clusters are distributed within the lattice according to the synthesis conditions; wherein the magnetism is predicted by a two-phase model.

In order to get a clear idea about the inhomogeneities, the specific heat (C) was measured for the temperature range of 10-150 K as shown in Fig.5(i). The low-temperature region from 10-50 K is fitted using the polynomial[40]: $C = \gamma T + \beta_3 T^3 + \beta_5 T^5 + \beta_7 T^7$ as shown in Fig.5(ii). The γ gives the coefficient of electronic specific heat due to free charge carriers. The higher order T terms are the lattice contribution arising from phonons. The obtained values are γ=59.5 $mJmol^{-1}K^{-2}$ for the linear term, β_3=0.694 $mJmol^{-1}K^{-4}$, β_5=-2.54x10^{-4} $mJmol^{-1}K^{-6}$ and β_7=3.69x10^{-8} $mJmol^{-1}K^{-8}$. The high value of the electronic linear contribution to the low-temperature specific heat could be an indication of the coexistence of FM metallic and charge ordered state.[44] A higher value of γ is obtained for materials having FSC with GP.[40,43,44]

The electron spin resonance spectra obtained at 100 K, 170 K, and 300 K are shown in Fig.5(iii). ESR is highly sensitive to trivial magnetic correlations and is widely used for analyzing magnetic properties of manganites.[55-57] The ferromagnetic resonance signals, seen in the enlarged low field region of ESR spectra as shown in Fig.5(iv) clearly show the presence of FSCs. The coexistence of PM resonance and FM resonance (FMR) signal is an indication of co-existence of PM and FM clusters.[57]

Conclusions

In the present study, the disordered, orthorhombic La_2FeMnO_6 is found to possess double transition at T_{C1}=60 K and, T_C=425 K. The inverse susceptibility show a sharp downturn with temperature, below T*=570 K, as an indication of the occurrence of FSCs/GP. The oxidation states of cations are +3 (for Fe and Mn), and the effective PM moment is obtained as 6.5 μ_B / F.U. Fe^{3+}-O-Mn^{3+}, Fe^{3+}-O-Fe^{3+} and Mn^{3+}–O–Mn^{3+} superexchange interactions, and Mn^{3+}–O–Mn^{3+} dynamic FM interactions could be present in the system. These competing interactions are responsible for the occurrence of glassy like transition at 60 K and Griffiths-like phase at higher temperatures. The total thermo-magnetic picture of La_2FeMnO_6 is as follows. At T_C^R= 18 K, random dilution of FM phases starts due to the transition of some of the magnetic phases. The FM clusters within the matrix interacts with each other and these clusters will undergo spin flipping with time and enters into a Griffiths-like phase above T_C^R. At T_{C1}=60 K, most of the FM phase will undergo magnetic transition into PM state and at T_C=425 K, another magnetic transition occurs. Even though the T_C has reached, some of the FM clusters remain in the PM matrix and eventually transform completely into a PM state at T^*= 570 K, similar to a Griffiths-like phase. The Griffiths analysis yields a λ value 0.54 at 20 Oe and decreases to 0.29 at 200 Oe. Below T_C, the FM clusters present themselves as a matrix in which PM clusters are embedded. Above T_C, it seems the FM clusters are distributed within the PM matrix and eventually completely transforms to PM state. The intrinsic inhomogeneities associated with the structure, quenched disorder related to the B-site cations and the antisite boundaries cause the presence of FSCs. The coefficient of low temperature electronic specific heat is as high as γ=59.5 $mJmol^{-1}K^{-2}$, and such a high value can be argued to be responsible for FSCs. The electron spin resonance spectra show ferromagnetic resonance signals pointing the possibility of the presence of FSCs at room temperature. Normally, magneto-transport properties co-exist with GP, which can be explored in our future research, and the material is a promising candidate for room temperature applications. The coexistence of functionalities like FM, FiM, GP, magnetotransport coupling, etc. in a single material is of great interest for both the scientific aspects and for practical applications.

Acknowledgement

Jasnamol P P is thankful to the University Grants Commission (UGC), India and P Neenu Lekshmi is thankful to the Council of Scientific and Industrial Research (CSIR), India for providing Senior Research Fellowship. S. Thomas acknowledge the financial support received from DST, India, via INSPIRE faculty award. M. R. Varma is pleased to acknowledge Kerala State Council for Science, Technology & Environment (KSCSTE) and CSIR, India granted project SURE (No. CSC0132) for financial support. The authors are thankful to Mr. Ajeesh P Paulose for the technical support.

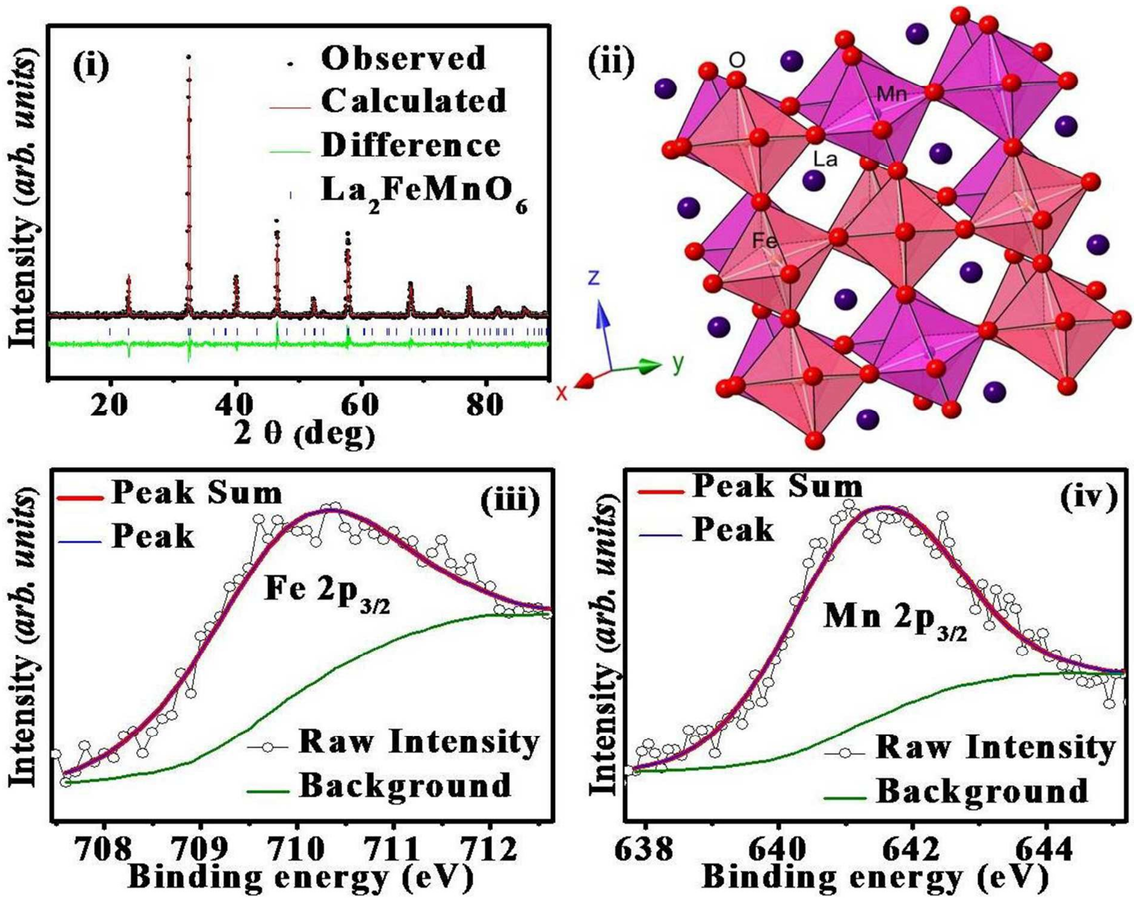

Fig.1(i) Observed, calculated and the difference XRD pattern of La_2FeMnO_6 obtained from Rietveld refinement.

Fig.1(ii) A small portion of the crystallographic structure of La_2FeMnO_6 crystal framed using CrystalMaker®

Fig.1(iii) XPS spectra of Fe $2p_{3/2}$ in La_2FeMnO_6 along with the fitted curves

Fig.1(iv) XPS spectra of Mn $2p_{3/2}$ in La_2FeMnO_6 along with the fitted curves

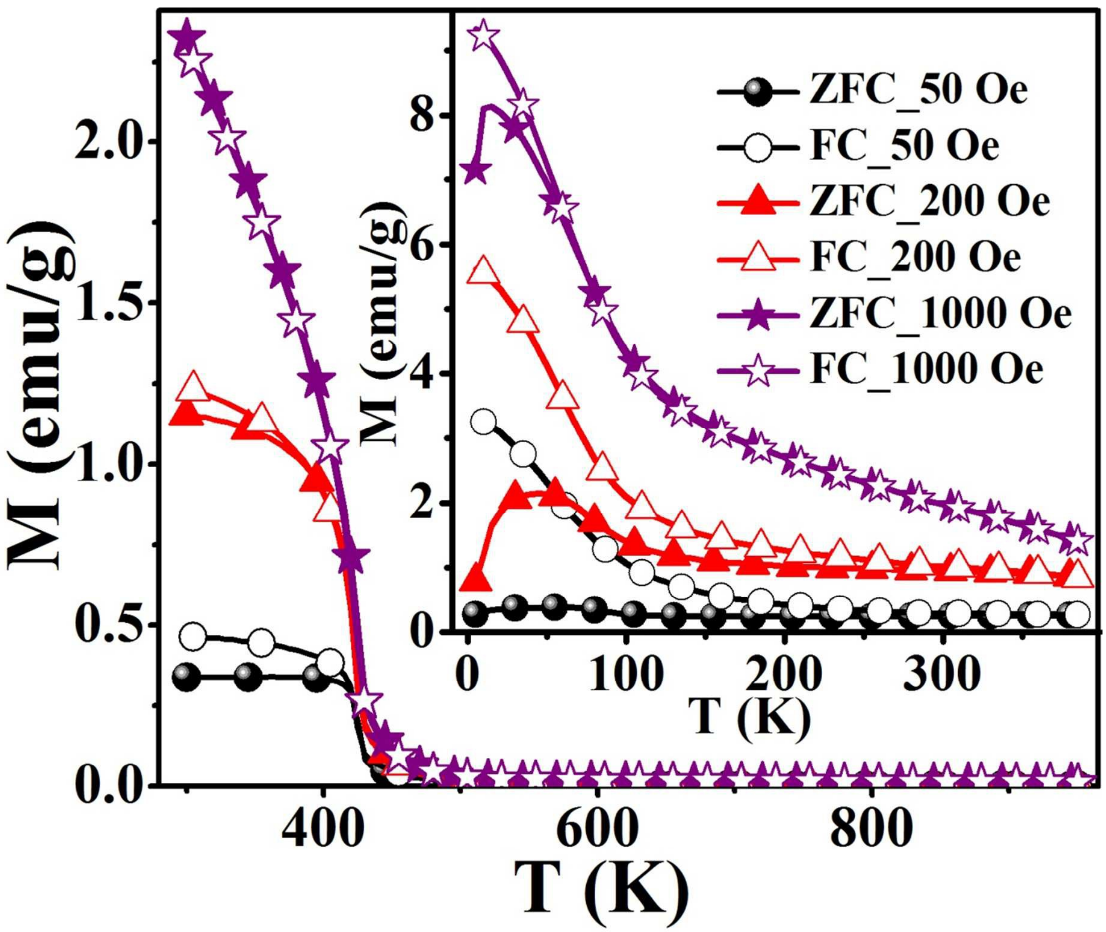

Fig.2. ZFC and FC curves at 50, 200, and 1000 Oe for 5-380 K
Fig.2.Inset: ZFC and FC curves at 50, 200, and 1000 Oe for 300-950 K

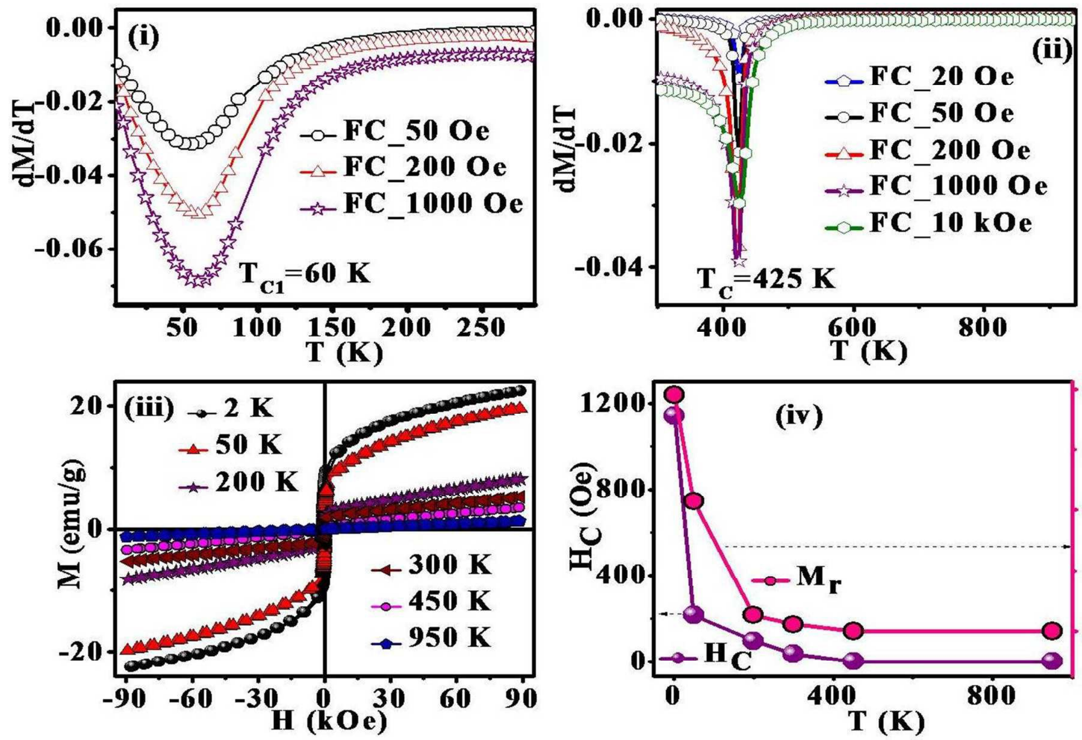

Fig. 3(i) Derivative of magnetization (FC) with respect to temperature vs. temperature for 5-300 K.

Fig.3(ii) Derivative of magnetization (FC) with respect to temperature vs. temperature for 300-950 K.

Fig. 3(iii) M-H curves recorded at different temperatures.

Fig. 3(iv) Variation of coercivity (H_C) and remanence (M_r) with temperature.

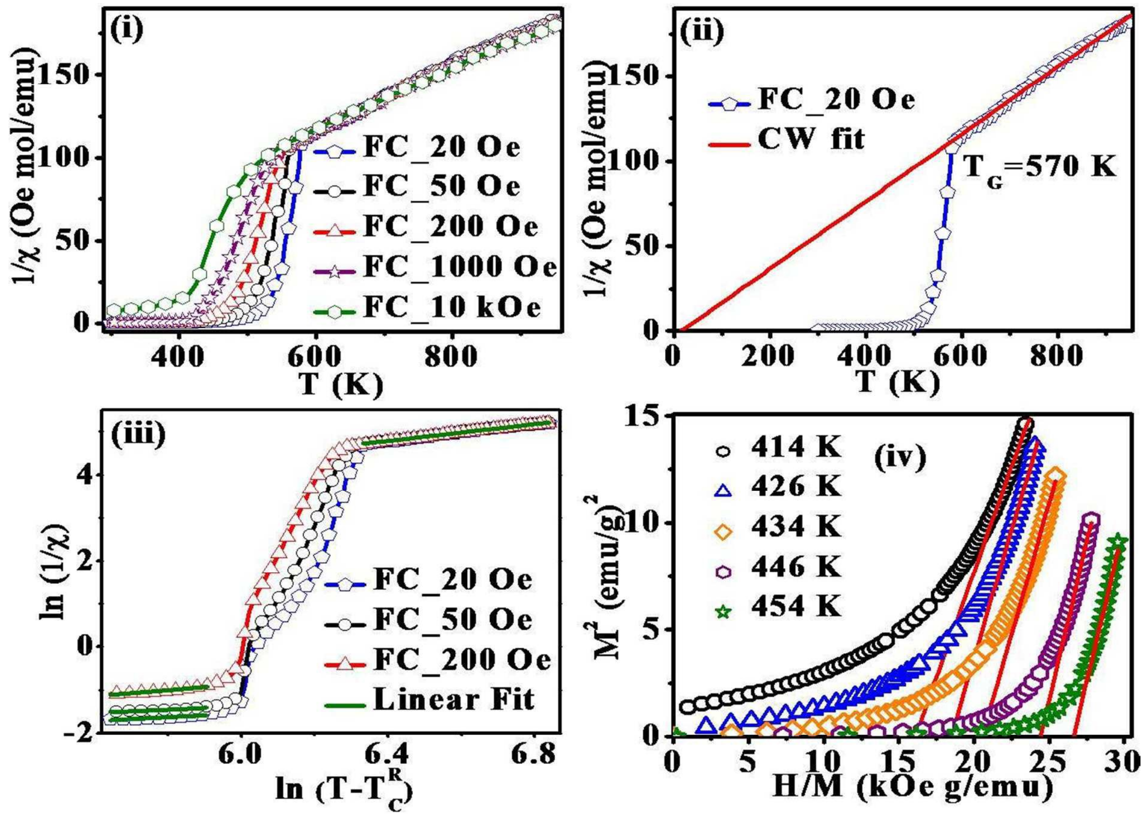

Fig.4(i) Temperature dependence of inverse susceptibility (FC) at various fields.
Fig.4(ii) CW fit (solid red line) on 1/χ (T) (FC) at 20 Oe
Fig.4(iii) ln (χ^{-1}) vs. ln (T-T_C^R) at 20, 50 and 200 Oe. The solid green line is the linear fit.
Fig.4(iv) The Arrot plot (M^2 vs. H/M) at different temperatures below and above T_C. The solid red line is the linear fit.

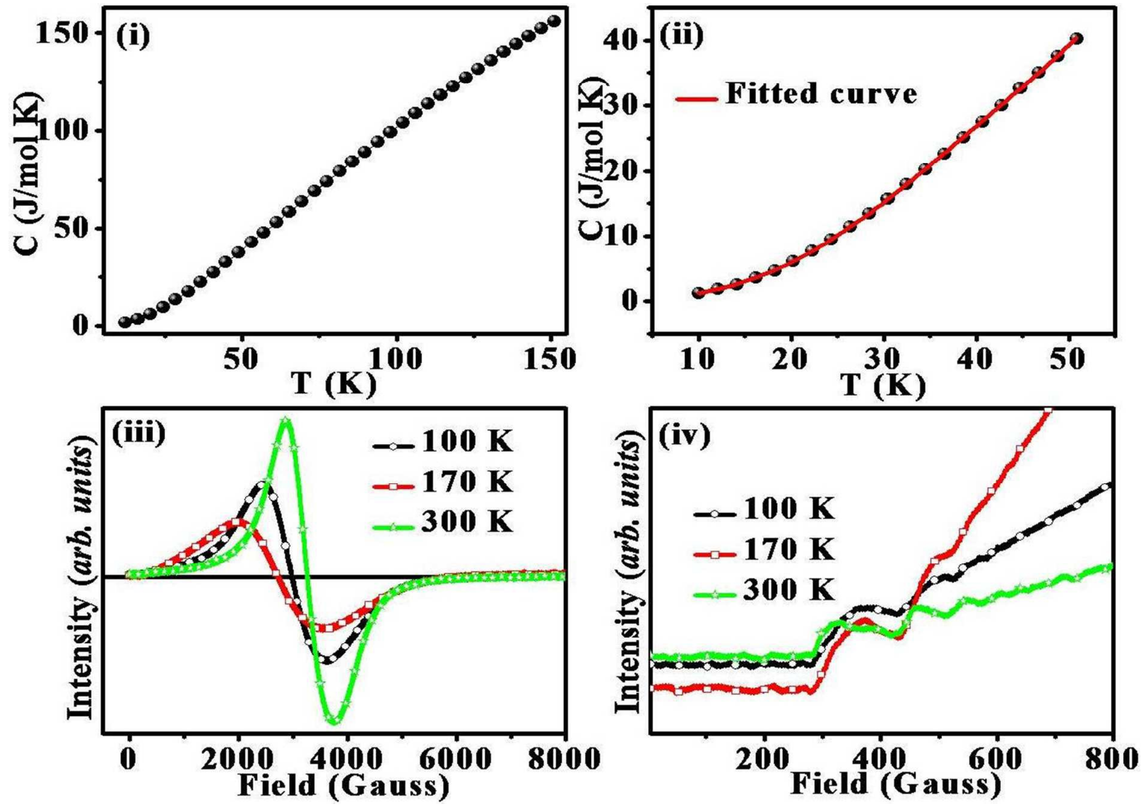

Fig.5(i) Specific heat (C) as a function of temperature.

Fig.5(ii) Low temperature specific heat C fit.

Fig.5(iii) ESR spectra of La_2FeMnO_6 at different temperatures.

Fig.5(iv) Enlarged low field region of ESR spectra showing FMR signals.

1. K.-I. Kobayashi, T. Kimura, H. Sawada, K. Terakura and Y. Tokura, Nature 395, 677 (1998).
2. P Baettig, C Ederer and N A. Spaldin, Phys. Rev. B 72, 214105 (2005).
3. M T. Anderson, K B. Greenwood, G A. Taylor, and K R. Poeppelmeiert, Prog. Solid State Chem. 22, 197 (1993).
4. Ll. Balcells, J. Navarro, M. Bibes, A. Roig, B. Martı´nez, and J. Fontcuberta, Appl. Phys. Lett. 78, 781 (2001).
5. R. von Helmolt, Meeker, B. Holzapfel, L. Schultz, and K. Samwer, Phys. Rev. Lett. 71, 2331 (1993).
6. M.-R. Li, M. Retuerto, Z. Deng, P. W. Stephens, M. Croft, Q. Huang, H. Wu, X. Deng, G. Kotliar, Javier Sanchez-Benitez, J. Hadermann, D. Walker, and M.Greenblatt, Angew. Chem. 127, 1 (2015).
7. P. Neenu Lekshmi, M. Vasundhara, Manoj Raama Varma, K.G. Suresh, M. Valant, Physica B 448, 285 (2014).
8. Y. Mao, J. Parsons and J. S. Mc Cloy, Nanoscale5, 4720 (2013).
9. R. Yadav, H. S. Nair, A. Kumar, S. Adiga, H. L. Bhat, S. M. Yusuf, and S. Elizabeth, J. Appl. Phys. 117, 093903 (2015)
10. P. Barrozo and J. Albino Aguiar, J. Appl. Phys. 113, 17E309 (2013).
11. J.M. D. Coey, M. Viret, and L. Ranno, Phys. Rev. Lett. 75, 3910 (1995).
12. J. M. D. Coey, M. Viret, Adv. Phys., 48, 167 (1999).
13. D. Choudhury, P. Mandal, R. Mathieu, A. Hazarika, S. Rajan, A. Sundaresan, U. V. Waghmare, R. Knut, O. Karis, P. Nordblad, and D. D. Sarma, Phys. Rev. Lett. 108, 127201 (2012)
14. Y. Guo, L.Shi, S. Zhou, J. Zhao, and W. Liu, Appl. Phys. Lett. 102, 222401 (2013).
15. J W Seo, E E Fullerton, F Nolting, A Scholl, J Fompeyrine and J-P Locquet, J. Phys.: Condens. Matter. 20, 264014 (2008).
16. P. Mondal, D. Bhattacharya, P. Choudhury, and P. Mandal, Phys. Rev. B 76, 172403, (2007).
17. J Kanamori, J. Phys. Chem. Solids. 10, 87, (1959).
18. P Ganguly, Bull. Mater, Sci., 3, 255 (1981).
19. Y. Wu, Z. Yu, S. Liu, J. Solid State Chem. 112, 157 (1994).
20. B. H. Toby, EXPGUI, a graphical user interface for GSAS, J. Appl. Cryst. 34, 210 (2001).
21. CrystalMaker Software Ltd, Oxford, England (www.crystalmaker.com).
22. Blomquist J., Helgeson U., Moberg L.C., Folkesson B., Larsson R., Inorg. Chim. Acta 69, 17 (1983)
23. Carver J.C., Schweitzer G.K., Carlson T.A., J. Chem. Phys. 57, 973 (1972)
24. Y Qian, H Wu, ErJun Kan, J Lu, R Lu, Y Liu, W Tan, C Xiao, and K Deng, J. Appl. Phys. 114, 063713 (2013).
25. O. F. de Lima, J. A. H. Coaquira, R. L. de Almeida, L. B. de Carvalho, and S. K. Malik, J. Appl. Phys. 105, 013907 (2009).
26. Zhi-Xian Wei, Yan Wang, Ji-Ping Liua, Cai-Mei Xiao, Wei-Wei Zeng, Mater. Chem. Phys. 136, 755 (2012).
27. D V Karpinsky, I O Troyanchuk and V V Sikolenko, J. Phys.: Condens. Matter. 19, 036220 (2007).
28. K. De, M. Thakur, A. Manna, S. Giri, J. Appl. Phys. 99, 013908 (2006).
29. K. De , R. Ray, R. N. Panda , S. Giri, H. Nakamura, T. Kohara, J. Magn. Magn. Mater. 288, 339 (2005).
30. S. D. Bhame, V. L. Joseph Joly, and P. A. Joy, Phys. Rev. B 72, 054426 (2005).
31. P. Barrozo, N. O. Moreno, J. A. Aguiar, Adv Mat Res, 975, 122 (2014).
32. K. Ueda, H. Tabata, and T. Kawai, Phys. Rev. B, 60, R12 561 (1999).

33. K. Ueda, Y. Muraoka, H. Tabata, and T. Kawai, Appl. Phys. Lett. 78, 512 (2001).
34. K. Yoshimatsu, K. Nogami, K. Watarai, K. Horiba, H. Kumigashira, O. Sakata, T. Oshima, and A. Ohtomo, Phys. Rev. B 91, 054421 (2015).
35. X.-D. Zhou, L. R. Pederson, Q. Cai, J. Yang, B. J. Scarfino, M. Kim, W. B. Yelon, W. J. James, H. U. Anderson and C. Wang, J. Appl. Phys. 99, 08 M918 (2006).
36. S.K. Giri, S.M. Yusuf, M.D. Mukadam, T.K. Nath, J. Alloys Compd., 591, 181 (2014).
37. A. K. Pramanik and A. Banerjee, Phys. Rev. B, 81, 024431 (2010).
38. W. Jiang, X. Z. Zhou, and G. Williams, Phys. Rev. B 77, 064424 (2008).
39. P. Tong, B. Kim, D. Kwon, T. Qian, S. Lee, S-W. Cheong, and Bog G. Kim, Phys. Rev. B 77, 184432 (2008).
40. H. S. Nair, D. Swain, Hariharan N. S. Adiga, C. Narayana, and S. Elzabeth, J. Appl. Phys. 110, 123919 (2011).
41. A. Shahee, K. Singh, R. J. Choudhary, and N. P. Lalla, Phys. Status Solidi B, 1 (2015).
42. S. Zhou, Y. Guo, J. Zhao, L.He, and L.Shi, J. Phys. Chem. C 115, 1535 (2011).
43. A. Slebarski, J. Goraus, and M. Fijałkowski, Phys. Rev. B 84, 075154 (2011)
44. C. L. Lu, K. F. Wang, S. Dong, J. G. Wan, J. M. Liu, and Z. F. Ren,J. Appl. Phys.103, 07F714 (2008)
45. S. Guo, D. P. Young, R. T. Macaluso, D. A. Browne, N. L. Henderson, J. Y. Chan, L. L. Henry, and J. F. DiTusa, Phys. Rev. Lett. 100,017209 (2008)
46. W. Jiang, X. Z. Zhou and G. Williams, Europhys. Lett.,84, 47009 (2008)
47. W. Jiang, X. Z. Zhou, and G. Williams, Phys. Rev. Lett. 99,177203 (2007)
48. C. Magen, P. A. Algarabel, L. Morellon, J. P. Araujo, C. Ritter, M. R. Ibarra, A. M. Pereira, and J. B. Sousa, Phys. Rev. Lett. 96,167201 (2006)
49. A. K. Pathak, D. Paudyal, W. T. Jayasekara, S. Calder, A. Kreyssig, A. I. Goldman, K. A. Gschneidner, Jr., and V. K. Pecharsky, Phys. Rev. B 89, 224411 (2014)
50. O. Chauvet, G. Goglio, P. Molinie, B. Corraze, and L. Brohan, Phys. Rev. Lett. 81,1102 (1998)
51. R. B. Griffiths, Phys. Rev. Lett. 23, 17 (1969).
52. A Moreo, M Mayr, A Feiguin, S Yunoki, and E Dagotto, Phys. Rev. Lett. 84, 5568 (2000)
53. Ren-Fu Y., Y. Sun, W. He, Qing-An Li, and Zhao-Hua C., Appl. Phys. Lett. 90, 032502 (2007)
54. V. Markovich, R. Puzniak, I. Fita, A. Wisniewski, D. Mogilyansky, B. Dolgin, G. Gorodetsky, and G. Jung, J. Appl. Phys. 113, 233911 (2013)
55. X.J. Liu, Z.Q. Li, A.Yu, M.L. Liu , W.R. Li, B.L. Li, P.Wu, H.L. Bai, E.Y. Jiang, J. Magn. Magn. Mater. 313, 354, (2007)
56. S. Zhou, L. Shi, H. Yang, and J. Zhao, Appl. Phys. Lett. 91, 172505 (2007)
57. J. Deisenhofer, D. Braak, H.-A. Krug von Nidda, J. Hemberger, R. M. Eremina, V. A. Ivanshin, A. M. Balbashov, G. Jug, A. Loidl, T. Kimura, and Y. Tokura, Phys. Rev. Lett. 95,257202 (2005)